

# Epidermal Electronics with Advanced Capabilities in Near-Field Communication

*Jeonghyun Kim, Anthony Banks, Huanyu Cheng, Zhaoqian Xie, Sheng Xu, Kyung-In Jang, Jung Woo Lee, Zhuangjian Liu, Philipp Gutruf, Xian Huang, Pinghung Wei, Fei Liu, Kan Li, Mitul Dalal, Roozbeh Ghaffari, Xue Feng, Yonggang Huang, Sanjay Gupta, Ungyu Paik,\* and John A. Rogers\**

We demonstrate materials, mechanics designs and integration strategies for near field communication (NFC) enabled electronics with ultrathin construction, ultralow modulus, and ability to accommodate large strain deformation. These attributes allow seamless, conformal contact with the skin and simultaneous capabilities for wireless interfaces to any standard, NFC enabled smartphone, even under extreme deformations and after/during normal daily activities. Detailed experimental studies and theoretical modeling of the coupled mechanical and electromagnetic responses of these systems establish foundational understanding of their behavior. These materials and device architectures have potential for utility in other types of radio frequency (RF) electronic systems and for use on other organs of the body.

Devices that offer capabilities in near field communication (NFC) appear increasingly in applications that span the banking,<sup>[1–3]</sup> medical,<sup>[1,2,4–7]</sup> military,<sup>[5,6,8]</sup> transportation<sup>[1,5,6]</sup>

and entertainment industries.<sup>[1]</sup> In fact, recent projections suggest that by the end of 2014, more than 150 million mobile devices (i.e. smartphones, laptops, etc) will support ability to interface to various NFC components, currently available in hard or flexible plastic packages and designed for use in free-standing forms or as stickers for mounting onto various objects.<sup>[1–3,5–9]</sup> More recent embodiments include wristbands,<sup>[4]</sup> bracelets<sup>[7]</sup> and tapes, as initial steps to wearable devices.<sup>[8,10]</sup> Here, we report materials and mechanics designs that allow NFC devices to be rendered in stretchable, ultrathin formats with physical properties that resemble those of the epidermis, for natural and imperceptible integration directly with the skin.<sup>[10]</sup> Thin NFC die connect to stretchable radio frequency (RF) antennas on low modulus elastomer substrates, to yield, ‘epidermal’ systems that mount on the skin like temporary transfer tattoos.<sup>[10–16]</sup> Experimental measurements of the resonant frequency and mechanical

J. Kim, A. Banks, Dr. S. Xu, Dr. K.-I. Jang, Dr. J. W. Lee, Dr. X. Huang, Prof. J. A. Rogers  
Department of Materials Science and Engineering  
Frederick Seitz Materials Research Laboratory  
University of Illinois at Urbana-Champaign  
Urbana, IL 61801, USA  
E-mail: jrogers@illinois.edu

J. Kim, Dr. J. W. Lee, Prof. U. Paik  
Department of Materials Science and Engineering  
Department of Energy Engineering  
Hanyang University  
Seoul 133–791, Republic of Korea  
E-mail: upaik@hanyang.ac.kr

H. Cheng, Prof. Y. Huang  
Department of Mechanical Engineering  
Civil and Environmental Engineering  
Center for Engineering and Health  
and Skin Disease Research Center  
Northwestern University  
Evanston, IL 60208, USA

Dr. Z. Xie, Prof. X. Feng  
Department of Engineering Mechanics  
Center for Mechanics and Materials  
Tsinghua University  
Beijing 100084, China

Dr. Z. Xie  
Department of Civil and Environmental Engineering  
Northwestern University  
Evanston, IL 60208, USA

Dr. Z. Liu  
Institute of High Performance Computing  
1 Fusionopolis Way, #16–16 Connexis  
Singapore 138632, Singapore

P. Gutruf  
Functional Materials and Microsystems Research Group  
School of Electrical and Computer Engineering  
RMIT University  
Melbourne, VIC 3000, Australia

Dr. P. Wei, M. Dalal, Dr. R. Ghaffari, Dr. S. Gupta  
MC10 Inc., Cambridge  
Massachusetts 02140, USA

F. Liu, K. Li  
Department of Engineering Mechanics  
Tsinghua University  
Beijing 100084, China



DOI: 10.1002/sml.201402495

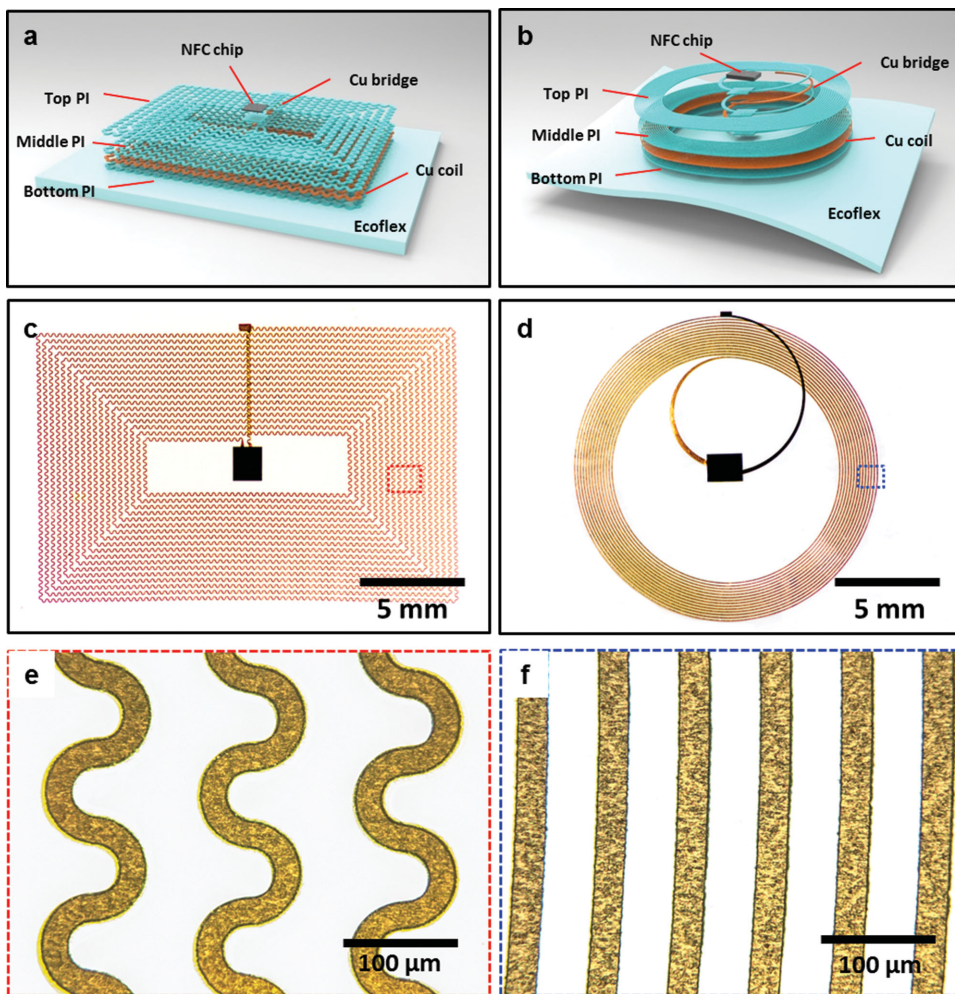


**Figure 1.** Schematic illustrations, pictures, and optical microscope images of skin-mounted NFC devices with two different types of coil. Exploded-view schematic illustrations of each layer of the skin-mounted NFC devices with (a) rectangular coil and (b) circular coil. (c, d) Photo images of the devices after NFC chip assembly. (e, f) Optical microscope images of each region of (c, d) indicated by (e) the red dashed box and (f) the blue dashed box.

properties compare favorably to results of theoretical modeling for two different device designs. Demonstrations of functional operation on the skin illustrate the capabilities.

**Figure 1** shows exploded view schematic illustrations (Figure 1a, b) and images (Figure 1c, d) of epidermal NFC devices with rectangular (20 mm × 14 mm) and circular (16 mm  $\phi$ ) coil designs. Both copper RF antennas resonate at frequencies near 13 MHz, where a thinned silicon integrated circuit die (50  $\mu$ m thick) serves as a standard NFC interface to smartphones and other devices. The coils include encapsulating layers of polyimide above and below to physically isolate the copper and to place it near the neutral mechanical plane. Contact pads at the ends of the coils allow connection to the NFC die using a modified flip-chip technique.<sup>[14]</sup> Addition of a thin stretchable encapsulating layer over the die completes the fabrication. Magnified views of representative regions of the coils appear in Figure 1e and 1f. The rectangular design exploits 19 turns of copper traces (5  $\mu$ m thick and 76  $\mu$ m wide) in filamentary serpentine shapes to provide stretchability. The circular coil includes 15 turns of copper traces with similar thicknesses and widths, but without the

serpentine configuration. Here, the overall curvature of the traces provides stretchability, as described subsequently. The NFC dies are located in the center regions of both coils, where they connect to the coils. Transfer to a supporting substrate and encapsulation with a uniform sheet of material completes the fabrication. For results on skin described here, a low modulus acrylic adhesive with thicknesses of  $\sim$ 25  $\mu$ m serves as the substrate. This thin, soft construction allows conformal contact with the skin via van der Waals interactions alone. The adhesive nature of the acrylic improves significantly the bonding strength, as described subsequently.<sup>[10,13,15]</sup>

**Figure 2** shows each type of device under three levels of uniaxial deformation up to 30% and corresponding results of three dimensional finite element analysis (FEA), where the color represents the maximum principal strain. In these experiments, a relatively thick support of a commercial, low modulus silicone material (Ecoflex, 2.5 mm thick, 0.069 MPa modulus) serves to simulate the skin. A tensile load in the horizontal direction was applied at the ends of the devices, as shown in Figure 2. For the case of rectangular design in Figure 2a, the serpentes change in geometry and the

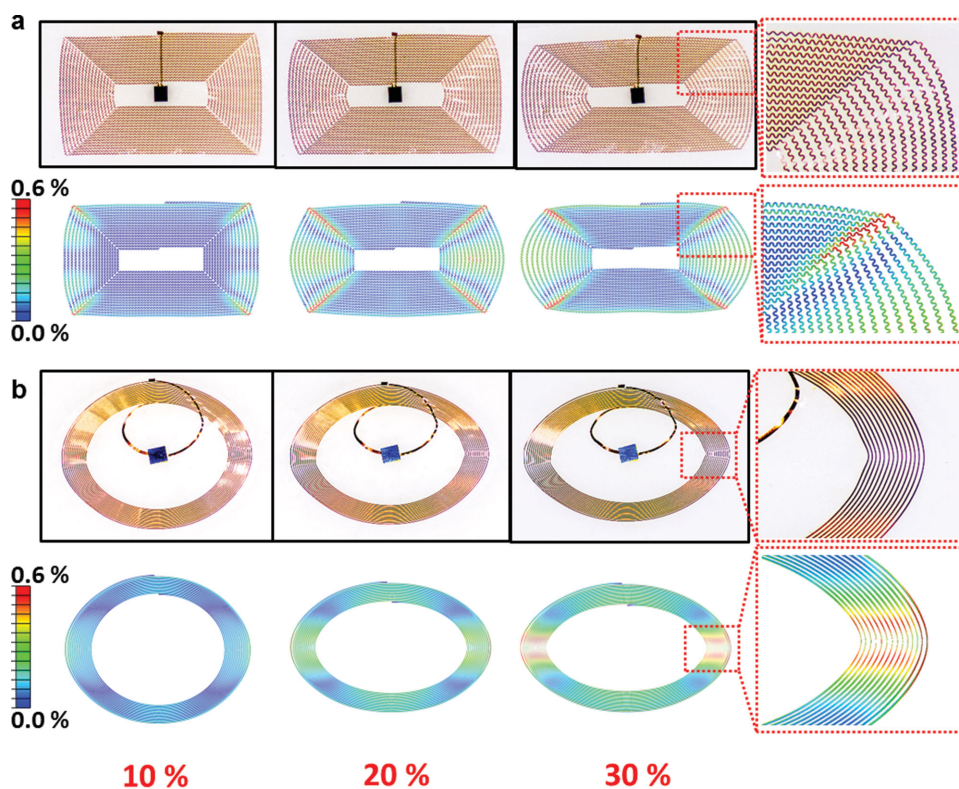


**Figure 2.** Photos of the NFC devices under four levels of uniaxial deformation and corresponding mechanic modeling results. (a) Photo images of rectangular coil under three levels of uniaxial deformation up to 30% and corresponding mechanical modeling results. (b) Photo images of circular coil under three levels of uniaxial deformation up to 30% and corresponding mechanical modeling results. The insets highlight a selected highly deformed region, both for modeling and experiment.

spacing between adjacent vertical lines increases as the strain increases. The horizontal lines undergo little change (e.g.,  $\sim 1\%$  for a stretching to 30%), as evidenced by the negligible maximum principal strains in these regions (Figure 2). In-plane bending plays a significant role in the mechanics. As shown in Figure 2, the maximum principal strain occurs along two diagonals of the rectangle, similar to strain concentrations that occur in the corner regions of conventional, solid structures. Assuming  $\sim 0.3\%$  yield and  $\sim 5\%$  fracture strains for the copper, the elastic and total stretchability of the rectangular design are predicted to be  $\sim 8\%$  and  $\sim 55\%$ , respectively. In the circular design of Figure 2b, in-plane bending dominates over out-of-plane buckling, such that the structure deforms into an elliptical shape upon uniaxial stretching. The predicted elastic stretchability is  $\sim 23\%$ . However, in this case, the total stretchability of the circular coil is limited by the geometry instead of the strain, since a circle would become a straight line upon uniaxial stretching of  $\sim 57\%$ . Overall, the results from FEA show patterns of deformation that are in good agreement with those in the experimental images.

Measurements using an impedance analyzer (4291A RF impedance/material analyzer, Hewlett Packard) with a commercial primary coil (Samsung Galaxy Note II; resonant frequency  $\sim 47.5$  MHz) over a frequency range of 10 to 16 MHz, reveal the key electromagnetic properties, as summarized along with corresponding results of modeling in **Figure 3**. The impedance and phase responses show behaviors in quantitative agreement with theory. The resonant frequencies

of the rectangular and circular devices are 12.9 MHz and 12.53 MHz, respectively, in their unstrained configuration as determined using the Min-phase method.<sup>[11,17]</sup> The relatively broad frequency response results from a modest Q factor, and is important in allowing operation that is robust to shifts in frequency that can occur due to mechanical deformations.<sup>[9,18]</sup> Measurements and modeling results for these shifts as a function of uniaxial stretching to strains of up to 30% appear in Figure 3e, f.

The deformed structures from FEA in Figure 2 were imported into electromagnetic (EM) simulation software (Ansys HFSS 13 User's guide, Ansys Inc. 2011) to determine the interactions between the primary and circular/rectangular coils. The magnetic field ( $B$ ) obtained numerically determines the inductance  $L$  according to  $L = \int B \cdot dS/I$ , where  $S$  is the in-plane area enclosed by the coil, and  $I$  is the current. Upon uniaxial stretching in the horizontal direction of the rectangle, the inner spacing of the vertical lines gradually increases due to unfolding of local serpentes (see Figure 2a). These dimensional changes increase the in-plane area enclosed by the coil, which can be represented as the ratio of the deformed to original areas, and can be written as (see SI for details).

$$\frac{S + \Delta S}{S} = (1 + \varepsilon)(1 - \nu\varepsilon), \quad (1)$$

where  $\varepsilon$  is the applied uniaxial strain, and  $\nu$  is the Poisson's ratio of the substrate. For 30% uniaxial stretching and  $\nu = 0.5$ ,

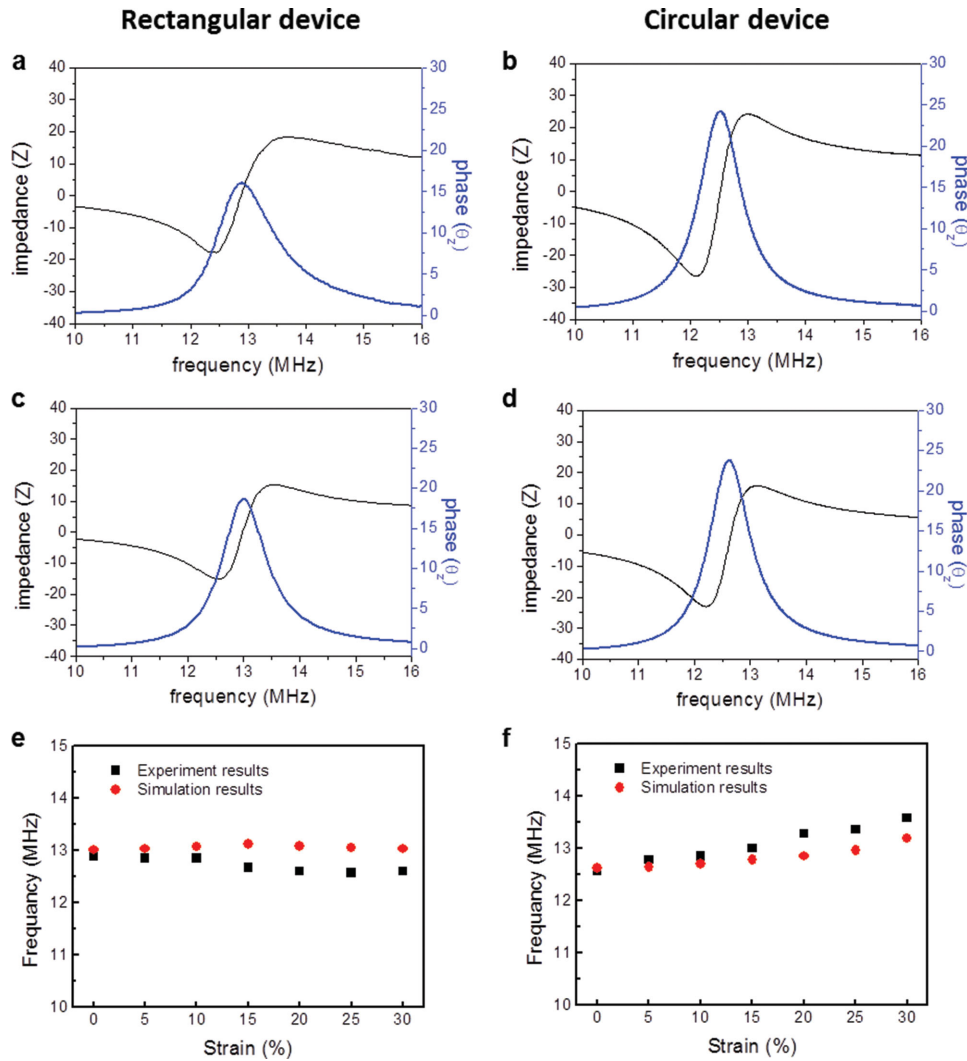


**Figure 3.** Experimental and modeling results of the NFC devices. (a, b) Frequency dependent impedance and phase responses, (c, d) corresponding electromagnetic modeling results. (e, f) Resonant frequency changes with uniaxial strain and corresponding modeling results of each device.

the enclosed area increases by 10.5%. Therefore, the inductance increases due to an increased magnetic flux, which leads to a decrease in the resonant frequency  $f_0 = (2\pi\sqrt{LC})^{-1}$  for a constant capacitance  $C$  of the NFC die, as shown in Figure 3e. For the circular coil, uniaxial stretching changes the shape to an ellipse and thereby decreases the in-plane area (Figure 2b) and increases the resonant frequency (Figure 3f). The ratio of the deformed to original areas for this case is given by (see SI for details)

$$\frac{S + \Delta S}{S} = \frac{1 + \varepsilon}{9} \left[ 5 - 7\varepsilon + 4\sqrt{(1 + \varepsilon)(1 - 2\varepsilon)} \right]. \quad (2)$$

For 30% uniaxial stretching, this enclosed area decreases by 16.4%. The calculated frequency shifts for both rectangular and circular cases are shown in Figure 3 as a function of the applied uniaxial strain. The results agree reasonably well with experiments, i.e., negative and positive frequency shifts for the rectangular and circular coils, respectively. In addition,

the smaller change of the enclosed area for the rectangular coil indeed correlates well with the smaller shift in frequency in Figure 3e, which suggests that the rectangular devices offer enhanced stability in operation (constant frequency) under strain. The circular devices, by comparison, have larger stretchability under uniaxial stretching (Figure 2b). All such results depend, of course, on the type of mechanical loading. For example, the rectangular coils give larger shifts in frequency and larger stretchability than circular coils under biaxial stretching.

The  $Q$  factors obtained from the electromagnetic simulations are  $\sim 8$  for the rectangular coil at the resonant frequency (13.02 MHz) of the device in the unstrained configuration, and  $\sim 14$  for the circular coil at the resonant frequency (12.62 MHz) of the device. Commercial coils that operate at similar frequencies typically have  $Q$  factors between 10 to 30.<sup>[19]</sup> Figure S4 shows the phase responses measured at different applied strains. The  $Q$  factor shows no consistent changes for deformations up to 30% (Figure S4c and d). The communication distance showed little change for the range of deformations

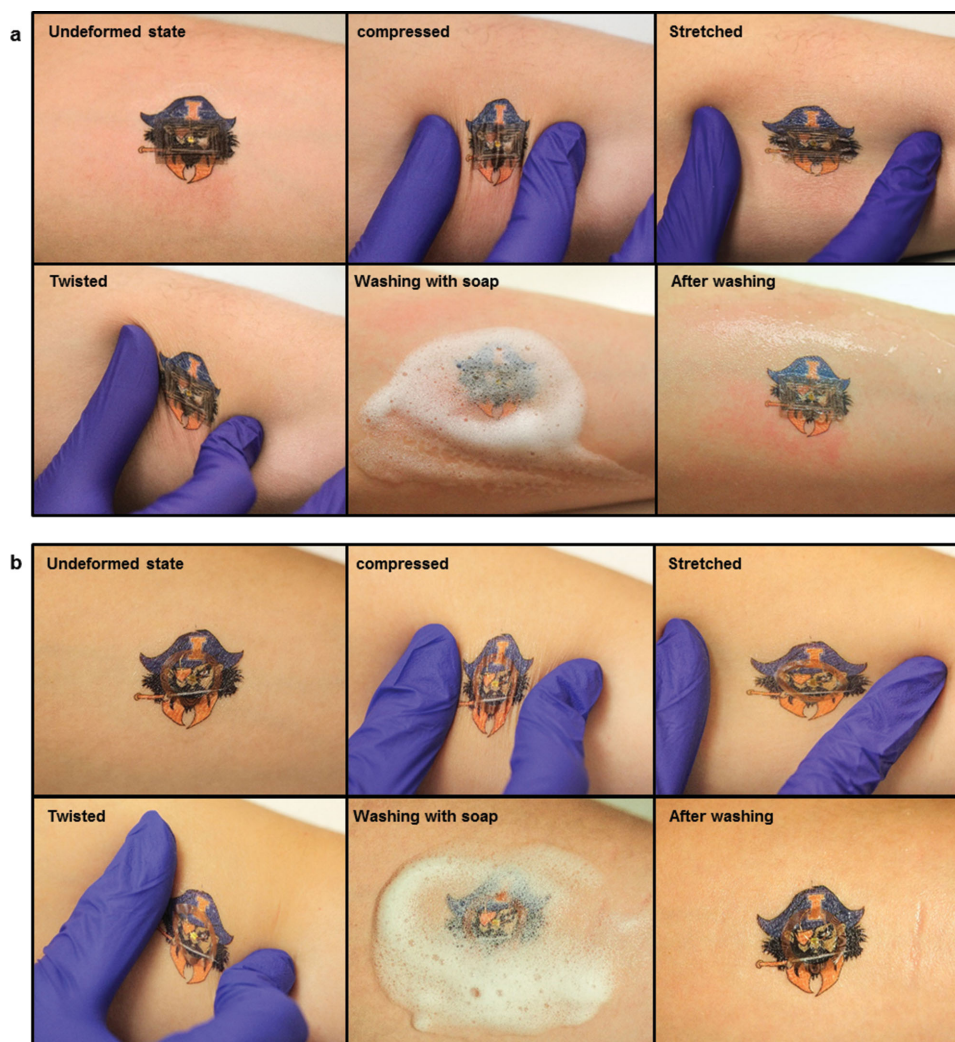


**Figure 4.** Images of the NFC devices during different deformation of the skin. (a) Photo images of the rectangular device under different kinds of deformation and washing with soap/water. (b) Photo images of the circular device under different kinds of deformation and washing with soap/water.

examined here. The higher bandwidth associated with lower Q factors help to ensure robust operation in the presence of shifts in resonant frequencies associated with mechanical deformation.

While mounted on the skin, both types of devices can communicate with any standard, NFC enabled smartphone. **Figure 4** provides images of devices on the forearm, with a commercial temporary transfer tattoo on top as an encapsulating layer. The mounting process involves retrieval of the devices using water-soluble tape followed by transfer onto a thin (25  $\mu\text{m}$ ), low modulus ( $\sim 0.017$  MPa) stretchable acrylic adhesive to ensure strong bonding to the skin, with minimal constraints on its natural motions. Application of the tattoo follows standard procedures outlined in the vendor instructions. The devices come into seamless, conformal contact with the skin and allow communication with a range of up to three centimeters, even under various states of deformation including compression, stretching, and twisting (See Figure 4 and video in SI). The low modulus, stretchable nature of these devices is qualitatively different and more

compatible with the natural mechanics of the skin than that of otherwise similar designs that use a standard, flexible backing made of Polyethylene terephthalate (PET) with thickness of 60  $\mu\text{m}$  (See **Figure 5a-c**, **Table 1**). The modulus, flexural rigidity, stretchability and water permeability (measured according to ASTM E96-95) of the acrylic substrate are  $\sim 0.017$  MPa,  $3.1 \times 10^{-11}$  N m,  $\sim 1400\%$  and  $515$   $\text{g}/\text{m}^2/\text{day}$  at room temperature (RT), respectively. The corresponding values for the PET substrate are  $\sim 2.5$  GPa,  $6.0 \times 10^{-5}$  N m,  $<3\%$  and  $6.4$   $\text{g}/\text{m}^2/\text{day}$  at RT. The devices function after/during normal daily activities, including washing with soap and water, immersion in water, exposure to vigorous sweating and other challenging scenarios. Devices remain operational for several days, depending on the wearer and their activities (including sports, exercise and swimming).

The materials, device designs and integration strategies introduced here enable state of the art NFC technology to be integrated in a seamless manner with the surface of the skin. The combined considerations in materials, electromagnetic and mechanical properties are essential to robust, functional

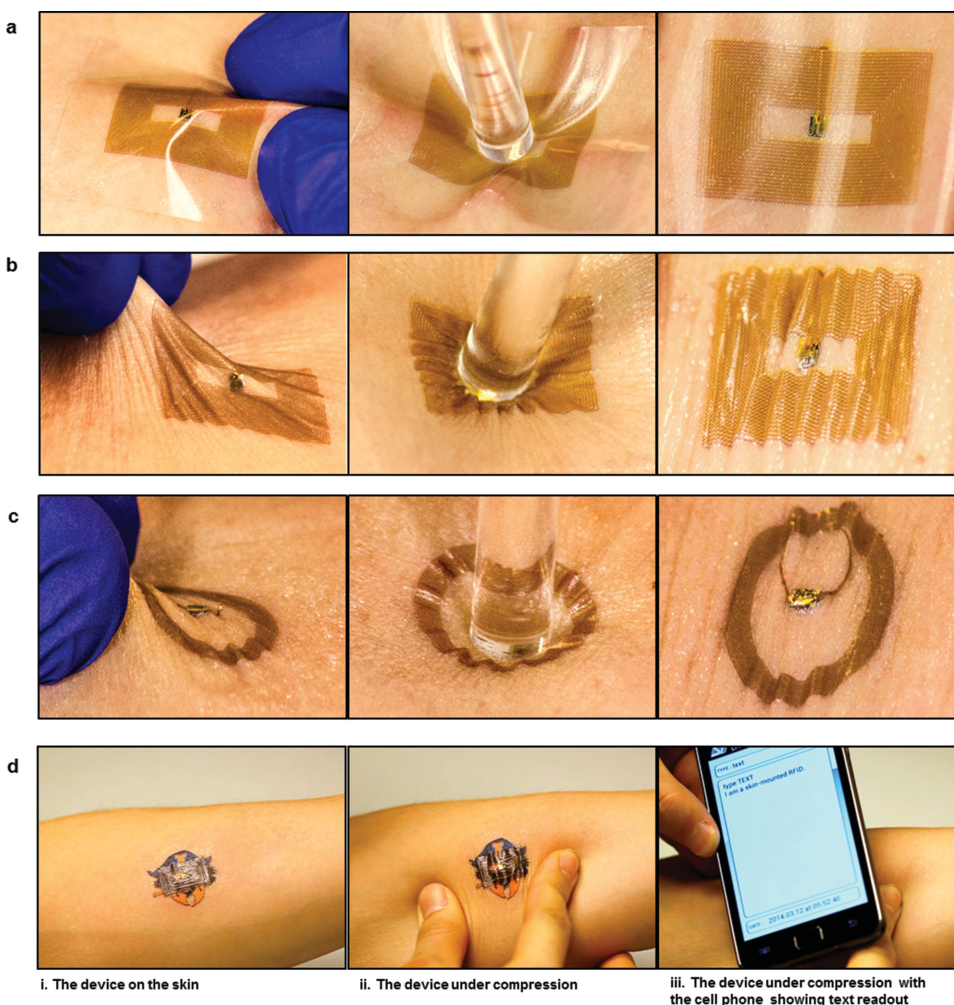


**Figure 5.** Demonstration of conformal skin contact and device functionality under stress. (a) shows a series of photos of devices mounted on a standard flexible substrate and their conformity with the skin. (b, c) show series of photo images that illustrates the conformity of an otherwise similar, but stretchable, device with the skin i. extreme pinch, ii. glass rod push, iii. extreme buckle. (d) shows a series of images that illustrates i. the device on the skin, ii. the device under compression, iii. the device under compression with the cell phone showing text readout.

operation and effective, skin-like properties. The same concepts should be applicable to other types of RF electronic systems and other organs of the body.

## Experimental Section

**Fabrication of the Coils:** The process begins with spin-casting of polydimethylsiloxane (PDMS, Sylgard 184) mixed at a 10:1 ratio of base to curing agent, by weight, onto a clean glass slide at 3000 rpm for 30 s, to form a film with thickness of  $\sim 10$   $\mu\text{m}$ .

Separately, spin-casting polyimide (PI2545, HD Microsystems) onto a 5  $\mu\text{m}$  thick Cu foil (Oak Mitsui Micro-thin series) at 3000 rpm for 30 s forms a film with thickness of 1.2  $\mu\text{m}$ . PDMS curing occurs on a hotplate at 110  $^{\circ}\text{C}$  for 30 min. Curing the PI involves baking on a hot plate at 150  $^{\circ}\text{C}$  for 5 min, followed by insertion into a vacuum oven at 250  $^{\circ}\text{C}$  for 1 h. The PI coated Cu foil is laminated onto the PDMS coated glass with the PI side in contact with the PDMS. The serpentine rectangular coil and circular coil are patterned by photolithography (AZ 4620 photo-resist, spin-casting at 3000 rpm for 30 s, baking at 110  $^{\circ}\text{C}$  for 3 min, UV irradiance for 300 mJ/cm<sup>2</sup>, development for  $\sim 40$  s with developer

**Table 1.** The physical properties of standard sticker tattoo and our stretchable device.

	Thickness [ $\mu\text{m}$ ]	Stretchability [%]	Young's Modulus of substrate [MPa]	Flexural rigidity of substrate [N m]	Water permeability of substrate [ $\text{g}/\text{m}^2/\text{day}$ at RT]
Standard sticker	150 $\mu\text{m}^{\text{a}}$ , 210 $\mu\text{m}^{\text{b}}$	<3	2500	$6.0 \times 10^{-5}$	6.4
Stretchable device	12 $\mu\text{m}^{\text{a}}$ , 60 $\mu\text{m}^{\text{b}}$	$\sim 55$	$\sim 0.017$	$3.1 \times 10^{-11}$	515

<sup>a)</sup>Antenna region; <sup>b)</sup>Chip region.

AZ 400K/deionized water solution of 1:2 volume ratio) and wet etching (CE-100 copper etchant, Transense). A layer of PI spin-cast over the entire coil at 2000 rpm for 30 s forms a uniform coating with thickness of approximately 2  $\mu\text{m}$ . Photolithography (AZ 4620) and oxygen plasma etching creates via holes through the PI. Mild etching in oxide remover (Flux, Worthington) eliminates the copper oxide at the base of the via holes. Electron beam evaporation forms a uniform layer of Cu (1  $\mu\text{m}$  thick) that is patterned by photolithography (AZ 4620) and wet etching (Copper etchant) to form the interconnecting bridge. Spin-casting yields an additional coating of PI (2  $\mu\text{m}$  thick). Electron beam evaporation of a 50 nm thick layer of  $\text{SiO}_2$  creates a hard mask in a geometry defined by photolithography (AZ 4620) and RIE etching (50 mT, 40 sccm  $\text{CF}_4$ , 100 W for 20 min). Oxygen plasma removes the exposed PI, leaving PI only in the regions of the coil. A buffered oxide etchant removes the  $\text{SiO}_2$  to complete the fabrication.

**Transfer and Chip Assembly:** A cellulose-based water-soluble tape (Grainger) serves as a means for retrieving the fabricated coil structure from its substrate. Bringing the cellulose tape, with the attached coil, into contact with the acrylic tape followed by removal of the cellulose by dissolution in water completes the transfer. A modified flip-chip method with an Indium/Ag based solder paste (Ind. 290, Indium Corporation;  $\sim 165^\circ\text{C}$  for 2 min in a reflow oven) enables attachment of thinned NFC chips (M24LR04E, ST Microelectronics, 50  $\mu\text{m}$  thick) onto contact pads on the coil. Addition of a small amount of elastomer (Ecoflex) encapsulates the die.

## Supporting Information

Supporting Information is available from the Wiley Online Library or from the author.

## Acknowledgements

This work was supported by the Global Research Laboratory (GRL) Program (K20704000003TA050000310) through the National Research Foundation of Korea (NRF) funded by the Ministry of Science, and used facilities in the Frederick Seitz Materials Research Laboratory and the Center for Microanalysis of Materials at the University of Illinois at Urbana-Champaign. Huanyu Cheng is a Howard Hughes Medical Institute International Student Research fellow. P. G. acknowledges an Australian Government Endeavour International Postgraduate Research Scholarship and the Australian Nanotechnology Network Overseas Travel Fellowship.

Y. H. acknowledges the support from NSF (DMR-1242240). We thank R. Dugan and D. Chandra of Google ATAP for useful discussions and interactions.

- [1] H. Du, *Int. J. Future Computer Commun.* **2013**, 351–354.
- [2] K. R. Foster, J. Jaeger, *IEEE Spectrum* **2007**, 44(3), 24–29.
- [3] V. Coskun, B. Ozdenizci, K. Ok, *Wireless Pers Commun* **2013**, 71(3), 2259–2294.
- [4] A. Lahtela, M. Hassinen, V. Jylha, *2008 2nd Int. Conf. Pervasive Computing Technol. Healthcare* **2008**, 229–232.
- [5] A. N. Nambiar, *Lect. Notes Eng. Comp.* **2009**, 1253–1259.
- [6] P. Najera, R. Roman, J. Lopez, *Security Commun. Networks* **2013**.
- [7] A. Marcus, G. Davidzon, D. Law, N. Verma, R. Fletcher, A. Khan, L. Sarmenta, *Proc. 1st Int. Workshop Near Field Commun.* **2009**, 30–35.
- [8] M. A. Ziai, J. C. Batchelor, *IEEE T. Antenn. Propag.* **2011**, 59(10), 3565–3571.
- [9] X. Yi, T. Wu, Y. Wang, R. T. Leon, M. M. Tentzeris, G. Lantz, *Int. J. Smart Nano Mater.* **2011**, 2(1), 22–38.
- [10] D. H. Kim, N. S. Lu, R. Ma, Y. S. Kim, R. H. Kim, S. D. Wang, J. Wu, S. M. Won, H. Tao, A. Islam, K. J. Yu, T. I. Kim, R. Chowdhury, M. Ying, L. Z. Xu, M. Li, H. J. Chung, H. Keum, M. McCormick, P. Liu, Y. W. Zhang, F. G. Omenetto, Y. G. Huang, T. Coleman, J. A. Rogers, *Science* **2011**, 333(6044), 838–843.
- [11] X. Huang, Y. H. Liu, H. Y. Cheng, W. J. Shin, J. A. Fan, Z. J. Liu, C. J. Lu, G. W. Kong, K. Chen, D. Patnaik, S. H. Lee, S. Hage-Ali, Y. G. Huang, J. A. Rogers, *Adv. Funct. Mater.* **2014**, 24(25), 3846–3854.
- [12] R. H. Kim, H. Tao, T. I. Kim, Y. H. Zhang, S. Kim, B. Panilaitis, M. M. Yang, D. H. Kim, Y. H. Jung, B. H. Kim, Y. H. Li, Y. G. Huang, F. G. Omenetto, J. A. Rogers, *Small* **2012**, 8(18), 2812–2818.
- [13] W. H. Yeo, Y. S. Kim, J. Lee, A. Ameen, L. K. Shi, M. Li, S. D. Wang, R. Ma, S. H. Jin, Z. Kang, Y. G. Huang, J. A. Rogers, *Adv. Mater.* **2013**, 25(20), 2773–2778.
- [14] S. Xu, Y. H. Zhang, L. Jia, K. E. Mathewson, K. I. Jang, J. Kim, H. R. Fu, X. Huang, P. Chava, R. H. Wang, S. Bhole, L. Z. Wang, Y. J. Na, Y. Guan, M. Flavin, Z. S. Han, Y. G. Huang, J. A. Rogers, *Science* **2014**, 344(6179), 70–74.
- [15] R. C. Webb, A. P. Bonifas, A. Behnaz, Y. H. Zhang, K. J. Yu, H. Y. Cheng, M. X. Shi, Z. G. Bian, Z. J. Liu, Y. S. Kim, W. H. Yeo, J. S. Park, J. Z. Song, Y. H. Li, Y. G. Huang, A. M. Gorbach, J. A. Rogers, *Nat. Mater.* **2013**, 12(10), 938–944.
- [16] T. Someya, *Stretchable Electronics*, Wiley-VCH, Weinheim, **2013**.
- [17] E. Sardini, M. Serpelloni, *Sensors* **2009**, 9(2), 943–960.
- [18] X. Huang, Y. Liu, K. Chen, W. J. Shin, C. J. Lu, G. W. Kong, D. Patnaik, S. H. Lee, J. F. Cortes, J. A. Rogers, *Small* **2014**, 10(15), 3083.
- [19] Y. Lee, RFID Coil Design, Microchip Technology Inc. AN678, technical note (accessible here: <http://ww1.microchip.com/downloads/en/AppNotes/00678b.pdf>), **1998**; pp.1–18.

Received: August 19, 2014  
 Revised: September 17, 2014  
 Published online: November 3, 2014